JACS
JOURNAL OF THE AMERICAN CHEMICAL SOCIETY
Article
pubs.acs.org/JACS

Furfuraldehyde Hydrogenation on Titanium Oxide-Supported Platinum Nanoparticles Studied by Sum Frequency Generation Vibrational Spectroscopy: Acid–Base Catalysis Explains the Molecular Origin of Strong Metal–Support Interactions

L. Robert Baker,*[,†,‡,§] Griffin Kennedy,[†,‡,§] Matthijs Van Spronsen,[⊥] Antoine Hervier,[†,‡,§] Xiaojun Cai,[†,‡,§] Shiyou Chen,[§] Lin-Wang Wang,[§] and Gabor A. Somorjai*[,†,‡,§]

[†]Department of Chemistry, University of California, Berkeley, California 94720, United States

[‡]Chemical Sciences Division and [§]Materials Science Division, Lawrence Berkeley National Laboratory, Berkeley, California 94720, United States

[⊥]Leiden Institute of Chemistry, Leiden University, P.O. Box 9502, 2300 RA Leiden, The Netherlands

ABSTRACT: This work describes a molecular-level investigation of strong metal–support interactions (SMSI) in Pt/TiO_2 catalysts using sum frequency generation (SFG) vibrational spectroscopy. This is the first time that SFG has been used to probe the highly selective oxide–metal interface during catalytic reaction, and the results demonstrate that charge transfer from TiO_2 on a Pt/TiO_2 catalyst controls the product distribution of furfuraldehyde hydrogenation by an acid–base mechanism. Pt nanoparticles supported on TiO_2 and SiO_2 are used as catalysts for furfuraldehyde hydrogenation. As synthesized, the Pt nanoparticles are encapsulated in a layer of poly(vinylpyrrolidone) (PVP). The presence of PVP prevents interaction of the Pt nanoparticles with their support, so identical turnover rates and reaction selectivity is observed regardless of the supporting oxide. However, removal of the PVP with UV light results in a 50-fold enhancement in the formation of furfuryl alcohol by Pt supported on TiO_2, while no change is observed for the kinetics of Pt supported on SiO_2. SFG vibrational spectroscopy reveals that a furfuryl-oxy intermediate forms on TiO_2 as a result of a charge transfer interaction. This furfuryl-oxy intermediate is a highly active and selective precursor to furfuryl alcohol, and spectral analysis shows that the Pt/TiO_2 interface is required primarily for H spillover. Density functional calculations predict that O-vacancies on the TiO_2 surface activate the formation of the furfuryl-oxy intermediate via an electron transfer to furfuraldehyde, drawing a strong analogy between SMSI and acid–base catalysis.

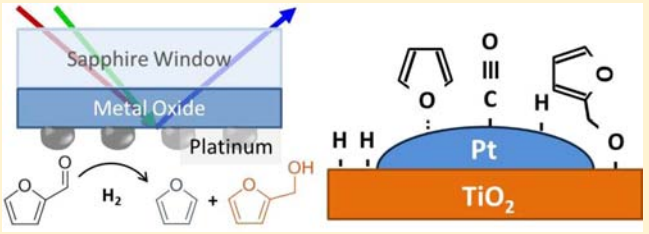

1. INTRODUCTION

Strong metal–support interactions (SMSI) refer to the ability of a seemingly inert oxide to have a dominant effect on the catalytic properties of a supported metal nanoparticle.[1−4] Tauster and Fung first used the term SMSI to refer to the dramatic loss of chemisorption sites observed for noble metal catalysts supported on titanium oxide after reduction.[2] In their studies, Tauster and Fung showed evidence for a strong bonding interaction between metal nanoparticles and a reduced titanium oxide support, and they used the term SMSI to refer directly to this bonding interaction.[4] However, because this metal–support interaction is closely linked to the catalytic properties of the metal involved, the definition of SMSI has since expanded to broadly refer to support-induced changes in the catalytic activity and selectivity of metal nanoparticles. SMSI plays an important role to enhance many catalytic reactions, including CO oxidation,[5−9] CO and CO_2 hydrogenation,[10,11] hydroformylation,[12] and partial hydrogenation reactions.[13−17] The ability of an oxide support to mediate the catalytic behavior of a supported metal nanoparticle is an important area in catalysis with both scientific and commercial significance. However, more than 30 years since its discovery, the mechanism of SMSI catalysis remains an open question.

A number of studies show that the support plays an important role in activating the C=O bond. A correlation of the catalyst activity for C=O bond hydrogenation with the Lewis acidity of the oxide empirically shows that charge transfer between the C=O bond and cationic sites in the oxide controls C=O bond activation.[11,18−20] This observation points out a similarity between SMSI and acid–base catalysis. In acid–base catalysis, the generation of ionic reaction intermediates determines the reaction rate and selectivity because the charged intermediate is highly active for a specific reaction pathway.[21−23] In SMSI the oxide appears to play a similar role: electron transfer between a reactant molecule and the oxide support leads to the formation of a charged reaction intermediate that may be highly selective to a specific reaction

Received: June 21, 2012
Published: August 7, 2012

   dx.doi.org/10.1021/ja306079h | J. Am. Chem. Soc. 2012, 134, 14208−14216

pathway. This hypothesis, which explains why SMSI can dramatically enhance the rate of a single reaction pathway, is confirmed in this study by direct observation of reaction intermediates on supported metal catalysts. These results show that SMSI catalysis is a subclass of acid−base chemistry where the flow of charge determines both reaction rate and selectivity.

In the current study, Pt nanoparticles supported on TiO_2 and SiO_2 serve as catalysts for furfuraldehyde hydrogenation. The Pt/SiO_2 catalyst serves a reference state, because SiO_2 is not SMSI active.[3] We investigate the effects of the support on the catalyst selectivity and correlate kinetic measurements with the surface intermediates observed by sum frequency generation (SFG) vibrational spectroscopy. SFG vibrational spectroscopy has been previously used to observe surface reaction intermediates on metal single crystals and shape controlled metal nanoparticles.[24−27] In this study, SFG is used for the first time to study, at a molecular level, how an oxide support controls the selectivity of a metal nanoparticle.

We find that initially the support has no effect on the reaction kinetics. This is because a layer of poly(vinylpyrrolidone) (PVP) encapsulates the Pt nanoparticles and insulates the Pt from the oxide support. However, by controlled removal of the PVP using UV light,[28] direct contact between the nanoparticles and the oxide support results in a new Pt/support interface. In the case of Pt/TiO_2, this interface leads to a 50-fold enhancement in the formation of furfuryl alcohol, while the Pt/SiO_2 interface has no effect on the reaction kinetics. By SFG we observe that a furfuryl-oxy intermediate forms on the TiO_2 as a result of a Lewis acid−base interaction with the furfuraldehyde molecule. This furfuryl-oxy intermediate is a highly active and selective precursor to furfuryl alcohol. Spectral analysis reveals that the Pt/TiO_2 interface is required primarily for H_2 spillover from the Pt. Density functional calculations identify O-vacancies on the TiO_2 surface as the catalytically active site and show that the barrier to C═O bond hydrogenation is dramatically decreased as a result of furfural bonding at the reduced Ti^{3+} sites surrounding an O-vacancy. This represents a detailed molecular understanding of the support-enhanced reaction mechanism for an SMSI catalyst and demonstrates a strong similarity between SMSI and acid−base catalysis.

2. EXPERIMENTAL SECTION

2.1. Catalyst Preparation. To study support effects, two-dimensional model catalysts were prepared by depositing Pt nanoparticles onto two different metal-oxide thin films. SiO_2 and TiO_2 served as the two supports. As synthesized, the Pt nanoparticles were encapsulated in a layer of PVP. This capping layer prevented actual contact between the Pt nanoparticle and the oxide support. However, by photodecomposition of the PVP, the Pt nanoparticles were brought into contact with the oxide support. By controlling the degree of contact between the particle and the support, the effect of the oxide-metal interface on catalytic activity and selectivity was studied.

As previously described, Pt nanoparticles were synthesized from chloroplatinic acid hexahydrate and PVP in a 1:4 mass ratio.[29] In a small beaker, 110 mg of chlorplatinic acid was dissolved in 10 mL of ethylene glycol. In a separate beaker, 440 mg of PVP was dissolved in 10 mL of ethylene glycol. Once in solution, the two mixtures were combined into a 50 mL two-neck round-bottom flask fitted with an Ar flow. The solution was purged under vacuum for 15 min. The vessel was then heated to 438 K for 1 h with vigorous mixing under a flow of Ar. The resulting nanoparticles were precipitated with acetone and washed three times with ethanol and hexanes. The nanoparticles were then suspended in chloroform for Langmuir−Blodgett (LB) deposition. Transmission electron microscopy (TEM) showed that the particles were 4.6 ± 2.8 nm.

Two substrates were used to support the nanoparticles: SiO_2 and TiO_2. For reaction studies, a Si(100) wafer with a 500 nm thermally grown oxide served as the SiO_2 support. The TiO_2 support consisted of a 50 nm TiO_2 thin film deposited on the SiO_2 substrate by electron beam evaporation. Following deposition, the TiO_2 thin film was annealed at 773 K in O_2. Analogous samples were prepared for sum frequency generation spectroscopic studies. For these samples, an optically transparent substrate was needed. A sapphire window rather than a Si wafer served as the substrate. A 50 nm thin film of SiO_2 or TiO_2 was deposited on the sapphire window by electron beam evaporation, again followed by annealing at 773 K in O_2 to ensure oxide stoichiometry.

The LB technique was then used to deposit a monolayer of the Pt nanoparticles onto the metal-oxide supports. This technique has been described previously in detail.[25,30] In short, a suspension of nanoparticles in chloroform is dispersed onto a water surface (18 MΩ). Time is given for the chloroform to evaporate, leaving a two-dimensional dispersion of nanoparticles on the water surface. The film is then compressed with a mobile barrier, and the surface pressure is monitored as a function of decreasing surface area. The surface pressure corresponds to the density of nanoparticles on the water. When the desired surface pressure is reached, a substrate is pulled out from under the surface of the water, and the film of nanoparticles is deposited onto the substrate. The final density of nanoparticles on the substrate can be controlled by controlling the surface pressure during deposition. A surface pressure of 14 mN/m was used for these studies, and films were deposited using a Nima 611 LB trough. Filter paper served as the surface tension probe. Prior to LB deposition the substrate was cleaned for 1 h in Nochromix solution. TEM showed that the area coverage for Pt on the substrate following LB was approximately 30%.

Immediately prior to reaction, the samples were exposed to UV light in air to photodecompose the PVP layer that encapsulated the nanoparticles. Two low-pressure mercury (Hg) lamps (Lights Sources Inc., model number GPH357T5VH/4P) were used as the UV source; the Hg lamp emitted two lines: 184 and 254 nm. The two lamps were positioned parallel to each other 2.5 cm apart in a clean Al box. The sample was positioned 1.2 cm below the lamps. By varying the time of UV exposure, it was possible to control the amount of PVP removed from the Pt nanoparticles. This cleaning is the combined effect of direct photodecomposition of the PVP as well as oxidation of the PVP by ozone produced by the 184 nm Hg line.[28]

2.2. Activity and Selectivity Measurements. A stainless steel batch mode reactor was used to determine the reaction rates and selectivity of furfuraldehyde hydrogenation for Pt supported on SiO_2 and TiO_2 with varying degrees of PVP cap removal. The catalyst was heated with a boron nitride substrate heater to a reaction temperature of 393 K. A metal bellows circulation pump provided gas mixing. Gas pressures were 1 Torr furfuraldehyde, 100 Torr H_2, and 659 Torr He. The furfuraldehyde was purified by freeze−pump−thaw cycles. Each catalyst was tested for 8 h and reaction products were monitored as a function of time using a gas chromatograph with a flame ionization detector.

To calculate a turnover frequency (TOF) for each catalyst, it was necessary to determine the number of Pt active sites. Because ethylene hydrogenation is insensitive to Pt structure[31] and support,[11] the number of active sites for each catalyst was determined by measuring the rate of ethylene hydrogenation and normalizing to a known TOF.[32] Ethylene hydrogenation was run on each catalyst following furfuraldehyde hydrogenation in a separate but identical reactor, and catalysts were stored under N_2 between reactions. The catalyst temperature for the ethylene reaction was 298 K, and gas pressures were 10 Torr ethylene and 100 Torr H_2 in a background of He.

Turnover frequencies for furfuraldehyde hydrogenation are based on the reaction rate, measured from a fit to peak area versus time, and normalized to the number of active sites as determined by ethylene hydrogenation. Selectivity measurements for furfuraldehyde hydrogenation are calculated as the TOF of a given product normalized to

dx.doi.org/10.1021/ja306079h | J. Am. Chem. Soc. 2012, 134, 14208−14216

the combined TOF of all products. Error bars represent 95% confidence intervals for these measurements.

2.3. Sum Frequency Generation Vibrational Spectroscopy. SFG is a second-order, nonlinear process that probes the $\mathbf{X}^{(2)}$ tensor. Because $\mathbf{X}^{(2)}$ is zero for centrosymmetric media, SFG is only sensitive to a break in inversion symmetry which usually occurs at a surface or interface. Consequently, SFG is useful for obtaining vibrational spectra of surfaces. In this study, SFG is used to obtain the vibrational spectra of molecules on the catalyst surface during reaction. Comparison of reaction intermediates on Pt nanoparticles supported on SiO_2 and TiO_2 demonstrates that a unique reaction pathway is active on the Pt/TiO_2 catalyst.

For SFG experiments, an active/passive mode-locked Nd:YAG laser (Leopard D-20, Continuum) produced a 20 ps pulse at a 20 Hz repetition rate. The fundamental output at 1064 nm was passed through an optical parametric generator/amplifier to generate a tunable infrared (IR) beam (2700−3600 cm^{-1}) and a second harmonic visible (VIS) beam (532 nm). The IR (100 μJ) and VIS (100 μJ) beams were spatially and temporally overlapped on the back surface of a sapphire window containing the Pt nanoparticles supported on SiO_2 or TiO_2 thin films. The VIS and IR beam were incident on the sample at 40° and 50°, respectively, relative to surface normal. The generated SFG signal was then collected and sent to a photomultiplier tube. A gated integrator was used to enhance the signal-to-noise. To collect a spectrum, the IR beam was scanned across the spectral range of interest. All experiments were performed in the ppp polarization combination.

The beams were directed onto the sample using a sapphire prism as shown in Figure 1. A solution of deuterated polystyrene (d8) in

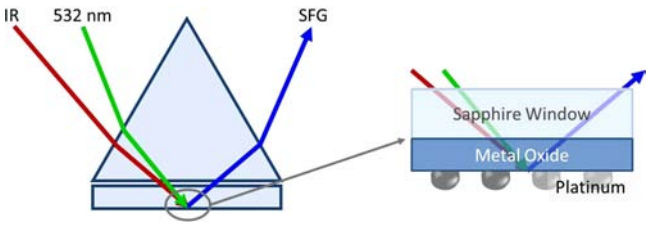

Figure 1. Diagram showing how a sapphire prism directed the VIS and IR beams onto the catalyst surface for SFG vibrational spectroscopy. The catalyst was prepared on the back side of a sapphire window and consisted of a thin film of either SiO_2 or TiO_2 acting as a support for Pt nanoparticles.

deuterated decalin (d18) served as an index matching liquid that did not interfere with transmission of the IR beam at the C−H stretch frequency. The catalyst surface was pressed into thermal contact with an aluminum heating block to heat the catalyst to reaction temperature. A recess in the heating block allowed for the flow of reaction gases across the catalyst surface. A metal bellows circulation pump provided gas mixing. A gastight seal was made between the sapphire window and the heating block using a Kalrez O-ring.

2.4. Density Functional Theory Calculations. The calculation is performed using the VASP code based on the density functional theory. For the exchange-correlation functional, the generalized gradient approximation (GGA) of Perdew−Burke−Ernzerhof (PBE) is used. The projector augmented-wave pseudopotentials are used with an energy cutoff of 400 eV for the plane-wave basis functions. To simulate the molecule absorption on the TiO_2 surfaces, a slab model is used with 6 Ti−O double layers (about 20 Å thick) and 10 Å vacuum layer, and a 1×2 supercell (about 10 Å × 8 Å) in the x−y plane. The Brillouin zone integration is carried out using 2×2×1 Monkhorst−Pack k-point meshes.

3. RESULTS AND DISCUSSION

3.1. PVP Cap Blocks Strong Metal−Support Interactions. Although many reaction products exist for furfuraldehyde hydrogenation depending on the pressure and temperature conditions,[17] we observed only four products which we break into two reaction pathways as shown in Scheme 1. The first pathway is decarbonylation to produce

Scheme 1

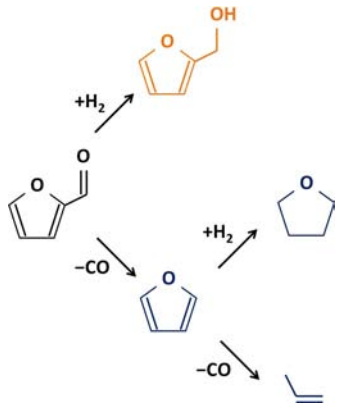

furan. Along this same pathway, furan can further hydrogenate to form tetrahydrofuran (THF) or further decarbonylate to form propylene.[27] The second reaction pathway is selective C═O bond hydrogenation to produce furfuryl alcohol.

Figure 2 demonstrates that the Pt/TiO_2 interface plays a major role in the production of furfuryl alcohol. Each plot shows the formation of reaction products as a function of time. Parts A and B show the results for PVP-capped Pt nanoparticles supported on TiO_2 and SiO_2, respectively. The PVP-capped particles show identical catalytic activity regardless of the support, indicating that the presence of the PVP cap prevents actual contact between the Pt nanoparticles and the oxide support. Parts C and D show the results for the same catalysts following removal of the PVP cap by UV treatment. The cleaned nanoparticles on TiO_2 show a 50-fold enhancement in the production of furfuryl alcohol which we attribute to the contact between the Pt and TiO_2 following the removal of PVP. However, the cleaned nanoparticles on SiO_2 show similar activity and selectivity to the capped nanoparticles, indicating that the Pt/SiO_2 interface does not play an important role in this reaction.

3.2. PVP Cap Removal by UV Cleaning. Figure 3A shows the C-to-Pt and the N-to-Pt atomic ratios of an LB film of nanoparticles as a function of UV treatment time measured by X-ray photoelectron spectroscopy (XPS). Both C and N signals decrease relative to the Pt signal with UV exposure, indicating that the PVP cap is being removed from the Pt nanoparticles. In this experiment the nanoparticles are supported on a doped Si wafer without any oxide layer to avoid charging during XPS measurements. The activity of the Pt nanoparticles increases by a factor of ∼5 with UV treatment time as determined by ethylene hydrogenation, indicating that more Pt sites become available as the cap is removed. The number of active sites after UV cleaning does not vary between TiO_2 and SiO_2 showing that the UV cleaning does not depend on the nanoparticle support. Figure 3B schematically depicts the effect of UV cleaning on the supported nanoparticles. As the PVP cap is removed, two important effects are observed: (1) the number of accessible Pt sites increases, so the activity of the catalyst for ethylene hydrogenation increases, and (2) the Pt nanoparticles come into contact with the oxide support. Electron microscopy shows that size and shape monodispersity of the UV-cleaned

dx.doi.org/10.1021/ja306079h | J. Am. Chem. Soc. 2012, 134, 14208−14216

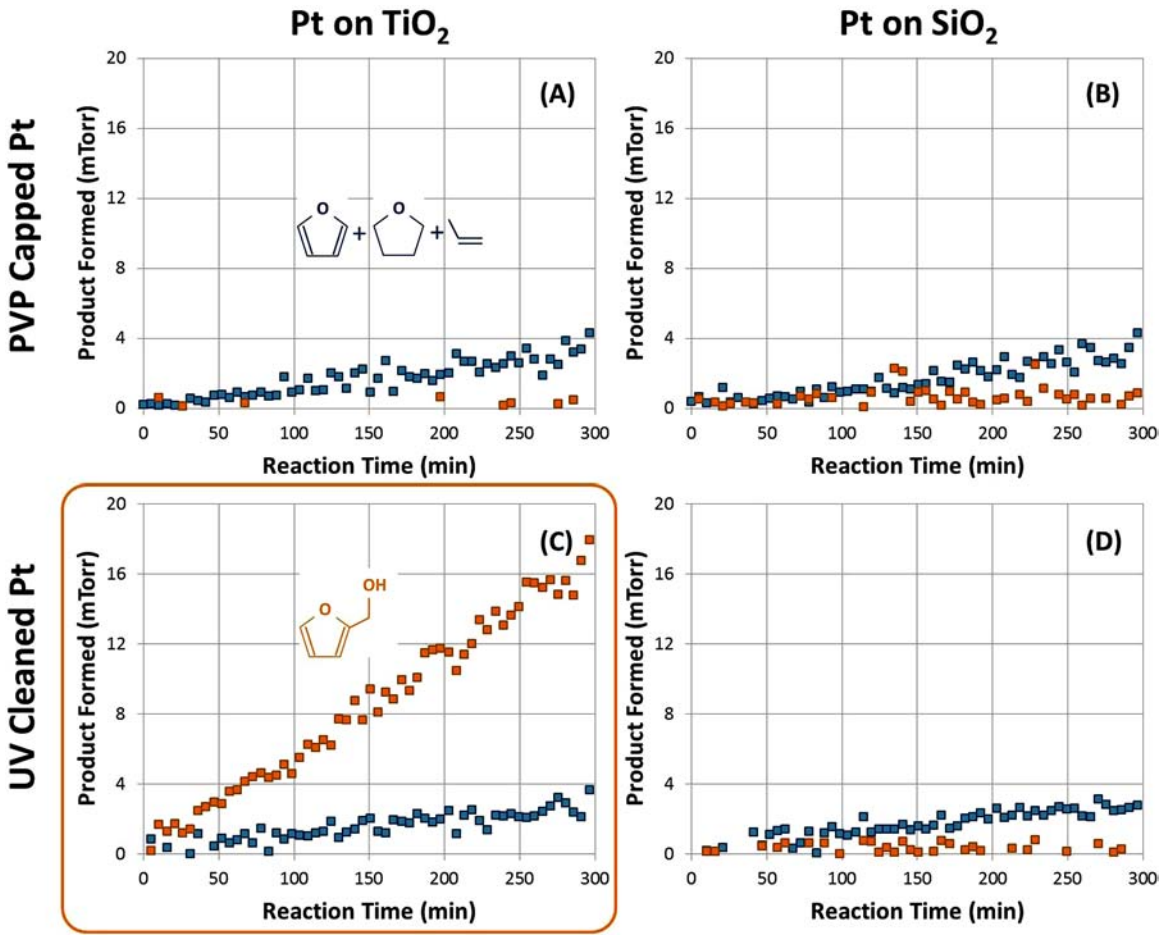

Figure 2. Formation of reaction products as a function of time on four Pt nanoparticle catalysts. (A,B) Results for PVP-capped Pt nanoparticles supported on TiO_2 and SiO_2, respectively. (C,D) Results for identical catalysts following 3 h UV cleaning to remove the PVP cap. Furfuryl alcohol is shown in orange, and decarbonylation products (i.e., furan, THF, and propylene) are shown in blue. The support has no effect on the activity or selectivity of the capped particles. However, following UV cleaning, the formation of furfuryl alcohol is selectively enhanced on the Pt/TiO_2 catalyst.

nanoparticles is lost during reaction because the uncapped nanoparticles are not as thermally stable as the PVP-capped nanoparticles.

3.3. Role of Pt/TiO_2 Interface on Reaction Kinetics and Selectivity. Figure 4 shows TOF of furfuraldehyde to decarbonylation products (i.e., furan, THF, and propylene) and to furfuryl alcohol as a function of UV treatment time for Pt on TiO_2 (A) and SiO_2 (B). The activity of each catalyst is normalized to the number of active sites measured by ethylene hydrogenation. As described above, this method is capable of measuring the number of Pt active sites without respect to Pt structure or support. Consequently, the changes in TOF with UV cleaning time shown in Figure 4 are already corrected for the increasing number of Pt sites as the PVP cap is removed. Initially, the PVP-capped Pt does not produce any furfuryl alcohol regardless of the support. However, as the Pt is brought into close interaction with the TiO_2 by UV cleaning, the activity for furfuryl alcohol production increases. Pt supported on SiO_2 does not produce any furfuryl alcohol outside of measurement error even after extensive UV cleaning. The data show that Pt activity for decarbonylation does not depend on the support, indicating that the oxide/metal interface has no effect on this reaction pathway.

It is interesting to note that for both supports the rate of decarbonylation decreases following 10 min UV cleaning. Although a rate increase is expected as the PVP is removed by UV cleaning, TOF shown in Figure 4 is already normalized to the number of available Pt sites. Consequently, this rate decrease following 10 min UV cleaning does not reflect a change in available Pt sites which is actually increasing. Rather the effect is due to a Pt size dependence for this reaction which results in a decreasing rate of furan formation as nanoparticle size increases.[33] The increase in nanoparticle size after 10 min UV cleaning is caused by nanoparticle agglomeration resulting from a loss in thermal stability following cap removal,[34] and this is confirmed by electron microscopy following reaction.

Figure 5 shows the selectivity of Pt supported on TiO_2 (A) and SiO_2 (B) as a function of UV treatment time. The selectivity of the Pt/TiO_2 catalyst for furfuryl alcohol increases with PVP removal, reaching ~90% after 180 min UV cleaning. This is a dramatic change in reaction selectivity changing from ~100% decarbonylation products on the capped nanoparticles to ~90% furfuryl alcohol on the cleaned nanoparticles. The Pt/SiO_2 catalyst shows no effect of PVP removal on the reaction selectivity and produces only decarbonylation products. These results suggest that the Pt/TiO_2 catalyst generates a unique reaction intermediate that is highly selective toward the formation of furfuryl alcohol. Below we demonstrate by SFG vibrational spectroscopy that the production of furfuryl alcohol correlates with a furfuryl-oxy intermediate that forms on TiO_2, and this furfuryl-oxy intermediate is the selective precursor to furfuryl alcohol.

dx.doi.org/10.1021/ja306079h | J. Am. Chem. Soc. 2012, 134, 14208−14216

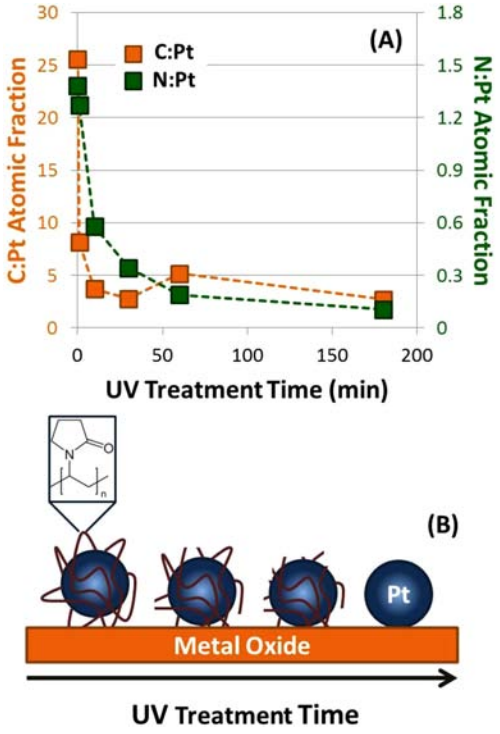

Figure 3. (A) C:Pt (orange) and N:Pt (green) atomic fractions for PVP-capped Pt nanoparticles as a function of UV cleaning time measured by XPS. Results indicate removal of the PVP cap from the Pt nanoparticles by UV photodecomposition. (B) Schematic showing the effects of UV cleaning on PVP-capped Pt nanoparticles. UV cleaning has two effects on the catalyst: (1) the number of available active sites per nanoparticle increases, and (2) the nanoparticles are brought into close contact with the support.

3.4. Probing Reaction Intermediates by SFG Vibrational Spectroscopy. Figure 6 shows SFG spectra of Pt/SiO_2 (A), TiO_2 without Pt (B), and Pt/TiO_2 (C) under reaction conditions following 180 min UV cleaning. The Pt/SiO_2 catalyst shows an intense stretch at 3030 cm^{-1}. This stretch is significantly lower frequency than the aromatic mode for the 5-membered furan ring which appears above 3100 cm^{-1}, and it has been previously assigned in furan hydrogenation as a vinylic stretch.[27] This indicates the presence of an unsaturated furan ring with broken aromaticity. A loss of aromaticity can occur in two ways: The first is partial hydrogenation of the ring to dihydrofuran (DHF) as has been previously observed for furan hydrogenation on Pt single crystals.[27] The second is by an interaction of the furan ring with the catalyst surface via the O atom. In the present study, GC measurements confirm that no DHF forms on this catalyst which is 60% selective to furan, 20% selective to THF, and 20% selective to propylene. Consequently, we assign this vinylic stretch to a furan ring bound to the Pt surface via the O atom as depicted in Figure 6A.

At lower temperatures we also observe a stretch at 2765 cm^{-1} (not shown) indicative of the aldehyde C−H stretch. However, this stretch disappears upon heating to 393 K due to decarbonylation of the furfuraldehyde to furan. This process results in CO deposition on the Pt surface which acts as a poison in the subsequent hydrogenation of furan to DHF, THF, or butanol. This explains the relatively low activity of this reaction pathway in furfuraldehyde hydrogenation compared to previous results for furan hydrogenation where at these pressures and temperatures, THF and butanol would be major products.[27] An additional weak stretch appears in Figure 6A at 2860 cm^{-1}. We assign this stretch to the symmetric CH_3 mode from π-bonded propylene which is a 20% product on this catalyst.

Figure 6B shows the spectrum of TiO_2 without Pt under reaction conditions. This spectrum shows two intense features. The first feature appears at 3,130 cm^{-1} and represents the aromatic stretch of the furan ring. The second feature is a located near 2920 cm^{-1} and represents the CH_2-symmetric mode. This spectrum correlates with a furfuryl-oxy intermediate resulting from furfuraldehdye bonding to the TiO_2 via the carbonyl O atom followed by the addition of a single H atom to the carbonyl C. This furfuryl-oxy surface intermediate is shown schematically next to the spectrum in Figure 6B and is the intermediate precursor to furfuryl alcohol formation. Although TiO_2 does not actively dissociate H_2, it is not surprising sufficient H atoms are present to produce a monolayer of

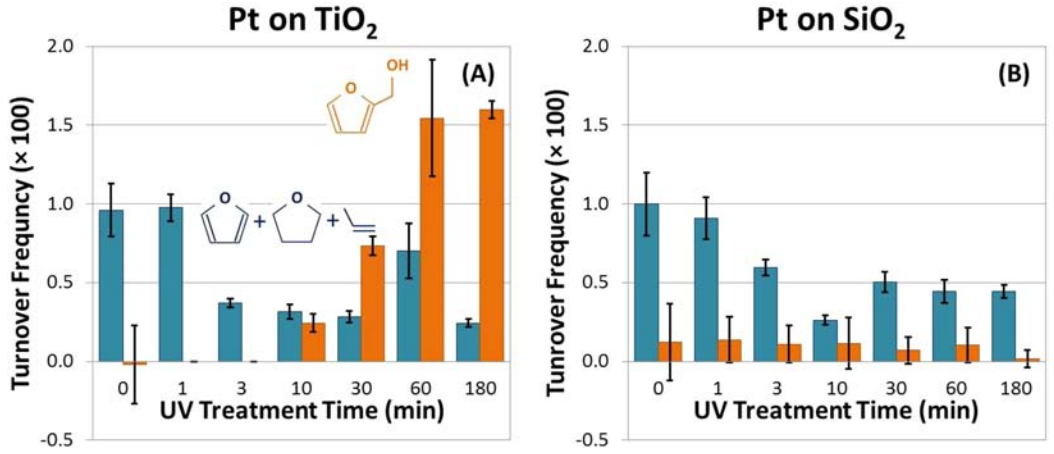

Figure 4. Turnover frequency (TOF) of furfuraldehyde by Pt supported on TiO_2 (A) and on SiO_2 (B) as a function of UV treatment time. Orange bars show the formation of furfuryl alcohol, representing selective C═O bond hydrogenation, and blue bars show the combined formation of furan, THF, and propylene, representing the decarbonylation pathway. All TOF values are normalized to the number of Pt actives sites measured by ethylene hydrogenation. Initially, no furfuryl alcohol is produced by Pt on either support. However, with UV cleaning, the formation of furfuryl alcohol is selectively enhanced on the Pt/TiO_2 catalyst.

dx.doi.org/10.1021/ja306079h | J. Am. Chem. Soc. 2012, 134, 14208−14216

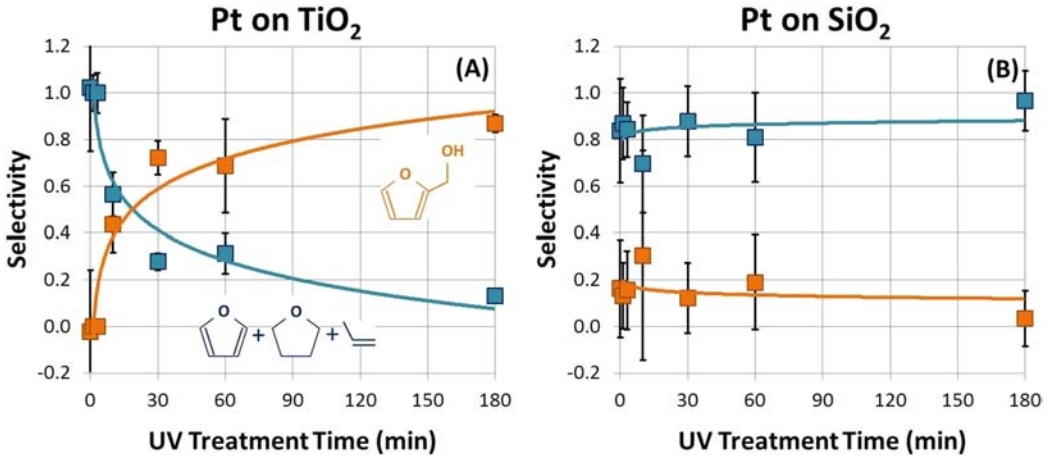

Figure 5. Selectivity for furfuraldehyde hydrogenation by Pt supported on TiO_2 (A) and on SiO_2 (B) as a function of UV treatment time. Furfuryl alcohol is shown in orange, and decarbonylation products (i.e., furan, THF, and propylene) are shown in blue. The selectivity of the Pt/TiO_2 catalyst changes dramatically with UV cleaning, going from 100% selectivity for decarbonylation products to ~90% selectivity for furfuryl alcohol. However, the Pt/SiO_2 catalyst is selective only for decarbonylation regardless of UV cleaning time.

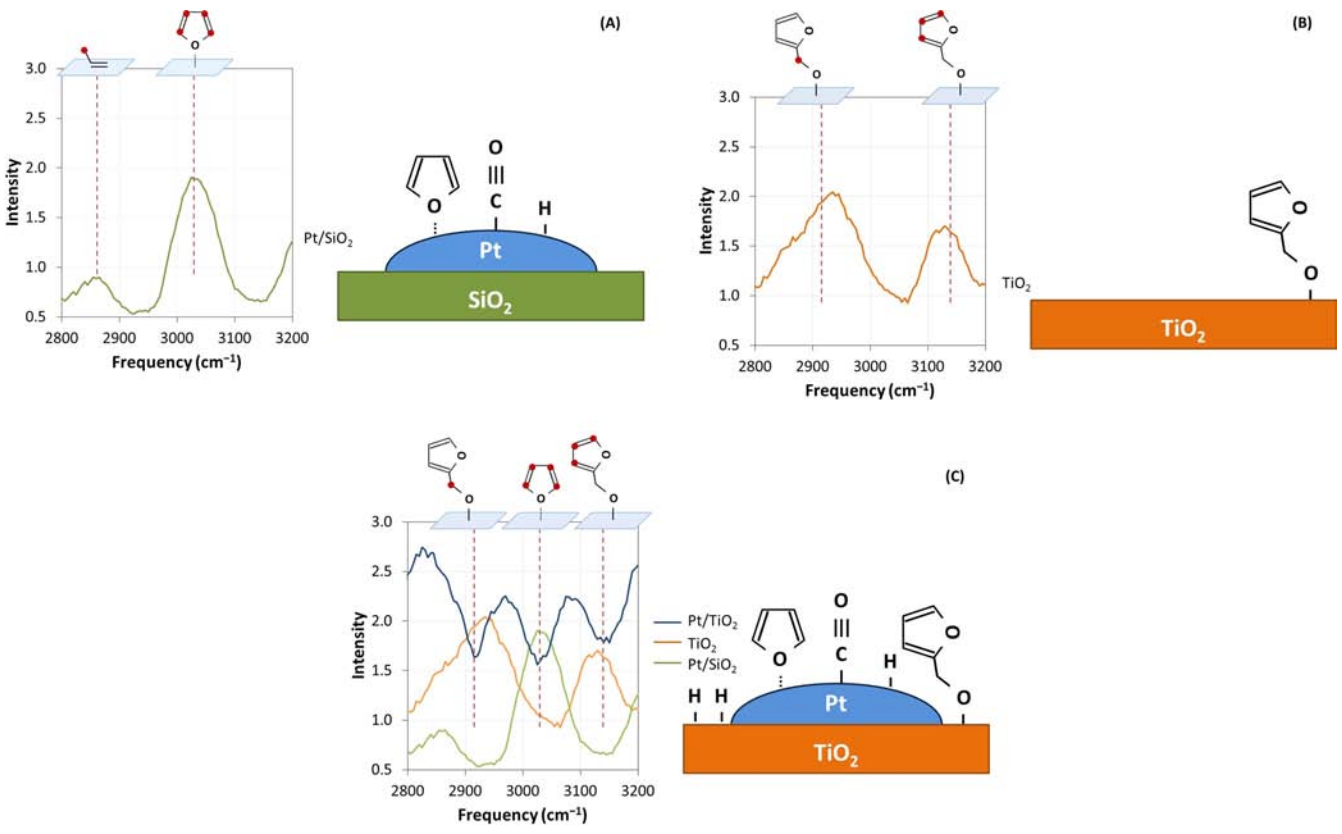

Figure 6. SFG spectra of Pt/SiO_2 catalyst (A), TiO_2 support without Pt (B), and Pt/TiO_2 catalyst (C) during reaction following 180 min UV treatment. Next to each spectrum a schematic depicts the surface intermediates represented in the spectrum, and red dots on the molecules above show the C−H bonds responsible for each vibrational mode. The Pt/SiO_2 catalyst (A) shows a strong feature at 3030 cm^{-1} representing the vinylic stretch of furan bound to the Pt surface via the O atom. This intermediate is the result of furfuraldehyde decarbonylation to CO and furan. A weaker stretch at 2860 cm^{-1} represents the CH_3-symmetric mode from π-bonded propylene which is a minor product on this catalyst. The TiO_2 support without Pt (B) shows a strong aromatic feature at 3130 cm^{-1} and a CH_2-symmetric stretch at 2,920 cm^{-1}. This spectrum represents a furfuryl-oxy intermediate resulting from furfuraldehdye bonding to the TiO_2 via the carbonyl O atom followed by the addition of a single H atom to the carbonyl C. This furfuryl-oxy surface intermediate is the precursor to furfuryl alcohol formation. The resonant features on the Pt/TiO_2 catalyst (C) overlap with the features already attributed to a furan intermediate on Pt and a furfuryl-oxy intermediate on TiO_2. This indicates that Pt has a similar reactivity when supported on either oxide, but that H spillover from Pt results in turnover of the furfuryl-oxy intermediate on TiO_2 to furfuryl alcohol. The nonresonant background is much higher for this sample compared to the Pt/SiO_2 and the TiO_2 without Pt, so the resonant modes appear as negative features against the high background.

dx.doi.org/10.1021/ja306079h | J. Am. Chem. Soc. 2012, 134, 14208−14216

furfuryl-oxy surface intermediates. This may be a result of slight H_2 dissociation at defect sites in the polycrystalline TiO_2 film, or the H atoms may come from hydroxyl groups that form on the TiO_2 surface in ambient or during UV cleaning. However, without a continual supply of H atoms from supported Pt nanoparticles, the TiO_2 substrate does not turnover.

Figure 6C shows the spectrum of the Pt/TiO_2 catalyst during reaction. In contrast to the spectra obtained on Pt/SiO_2 and TiO_2 without Pt, the nonresonant background of the Pt/TiO_2 sample is quite high, and the resonant modes appear as negative features against the high background. This effect, which is common in SFG, is a result of the phase mismatch between the resonant and nonresonant contributions of the spectrum. In the Pt/SiO_2 sample and TiO_2 sample without Pt, the nonresonant contribution to the spectrum is low, so any phase mismatch is not noticeable. However, the nonresonant component of the Pt/TiO_2 catalyst is much greater resulting in destructive interference with the resonant vibrations. The enhanced nonresonant signal in the Pt/TiO_2 catalyst is a result of H spillover from the Pt resulting in a reduced TiO_2 support. It is well known that in TiO_2, O-vacancies act as electron donors into mid-gap states of the reduced oxide which results in a greatly enhanced surface conductivity.[35] Because the nonresonant contribution to an SFG spectrum is largely the result of free electron motion at the surface of the substrate, it is not surprising that increased TiO_2 conductivity by H_2 reduction results in a dramatic enhancement of the nonresonant signal. This effect is reversible in O_2 as shown in Figure 7. Figure 7 plots the magnitude of the nonresonant signal in alternating H_2 and O_2 environments (100 Torr) for several catalyst samples. No furfuraldehyde is present during this experiment in which the catalyst is simply cycled between H_2 and O_2 atmospheres

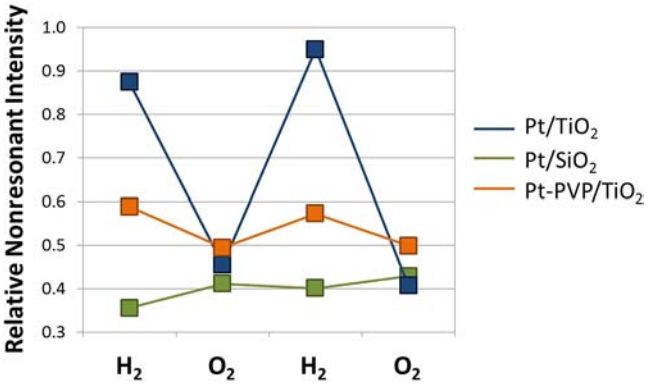

Figure 7. Relative nonresonant SFG intensity of a Pt/TiO_2 catalyst (blue), Pt/SiO_2 catalyst (green), and $Pt-PVP/TiO_2$ catalyst in alternating H_2 and O_2 environments (100 Torr) at 333 K. The Pt/TiO_2 and Pt/SiO_2 catalysts were UV-cleaned for 10 min (longer UV cleaning treatments do not change the results shown). The $Pt-PVP/TiO_2$ catalyst was not UV cleaned, so the PVP encapsulated the Pt nanoparticles and prevented contact between Pt and TiO_2. The nonresonant intensity is determined from the average intensity between 2700 and 2800 cm^{-1} where there are no resonant features. For the Pt/TiO_2 catalyst, the nonresonant background changes dramatically in H_2 and O_2. The enhanced nonresonant signal in H_2 is a result of H spillover from the Pt resulting in a reduced TiO_2 support, and this effect is reversible in O_2. The same effect is not observed for the Pt/SiO_2 catalyst and is only weakly observed for the $Pt-PVP/TiO_2$ catalyst before cap removal. This reflects the nonreducible nature of SiO_2 as well as the necessity of removing the PVP cap to enable H spillover from Pt to TiO_2.

and spectra are obtained in each. The catalyst cell is evacuated to <1 mTorr between gases. The nonresonant intensity is determined from the average intensity between 2700 and 2800 cm^{-1}. An effect on the nonresonant signal intensity is only significant for the Pt/TiO_2 catalyst following UV cleaning. The same effect is not observed for the Pt/SiO_2 catalyst and is only weakly observed for the $Pt-PVP/TiO_2$ catalyst before cap removal. This reflects the non-reducible nature of SiO_2 as well as the necessity of removing the Pt capping agent to enable H spillover to the TiO_2.

The resonant components of the Pt/TiO_2 spectrum during reaction correlate closely with the features observed on the Pt/SiO_2 and the TiO_2 samples, and the Pt/TiO_2 spectrum appears to represent a combination of the spectrum on Pt and the spectrum on TiO_2 as shown in Figure 6C. This indicates that Pt has a similar reactivity when supported on either oxide, but that H spillover from Pt results in turnover of the furfuryl-oxy intermediate on TiO_2 to furfuryl alcohol. As shown above by kinetic measurements, this reaction pathway is ~10 times faster than the decarbonylation reaction pathway which occurs only on Pt. This result demonstrates a striking similarity between SMSI and acid–base catalysis where both processes begin by formation of a unique reaction intermediate that acts as a highly active intermediate in a selective reaction pathway. In the case of SMSI, the TiO_2 support activates the furfuraldehyde molecule to form the highly selective furfuryl-oxy intermediate. The role of the crucial Pt/TiO_2 interface is simply to enable H spillover to this active intermediate.

3.5. Charge Transfer from TiO_2 to Furfuraldehyde. Density functional theory (DFT) calculations indicate that O-vacancies on the reduced TiO_2 surface are the catalytically active sites. Furfuraldehyde binding on the [101] surface of anatase TiO_2 is discussed here; binding on other low-energy surfaces was considered with similar conclusions. When there is no O-vacancy on the surface, the calculations show that the furfuraldehyde molecule does not bind with either Ti cations or O anions on the surface. However, when there is an O-vacancy on the surface, furfuraldehyde binds to one of the two Ti cations closest to the vacancy site, as shown in Figure 8, and the energy of the system decreases by 1.35 eV. The significant energy decrease associated with the binding can be understood considering that the Ti cations near the oxygen vacancy are in the reduced Ti^{3+} state, so one electron is occupying a high-energy mid-gap state near the conduction band. The binding of furfuraldehyde molecule oxidizes this cation to a Ti^{4+} state as one electron transfers to the furfuraldehyde molecule. The contour in Figure 8 shows the charge transfer during the binding process. The electron transfers from the area around the Ti^{3+} cation (shown by green contour) to the C=O bond (shown by blue contour). As a new Ti–O bond is formed, the original C=O double bond is changed into a C–O σ bond.

In the final surface binding state, the O atom in the furfuraldehyde molecule is coordinated by Ti and C and is in a stable full-shell state. However, the negative charge localized around the C atom represents a dangling bond, which is very reactive for H binding. A direct calculation shows the energy decreases by 0.2 eV when one H atom leaves the Pt surface and binds with this reactive C atom. Consequently, this step is fast and results in the steady state coverage of furfuryl-oxy intermediates on TiO_2 observed by SFG. This model of furfuraldehyde activation at O-vacancy sites in TiO_2 is also consistent with the experimental data showing that SMSI activity correlates with H spillover which occurs only for the

dx.doi.org/10.1021/ja306079h | J. Am. Chem. Soc. 2012, 134, 14208–14216

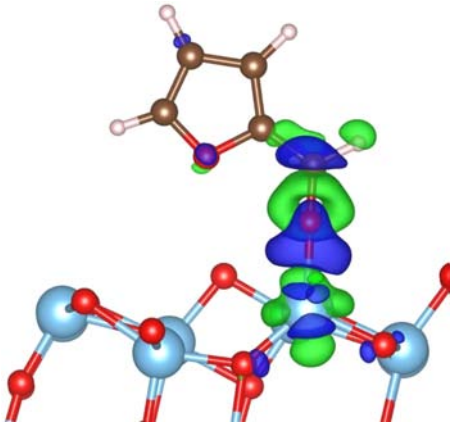

Figure 8. Structure plot of a furfuraldehyde molecule binding to a Ti cation near an O-vacancy site on anatase TiO_2 (101), and the charge transfer induced by the surface binding interaction. The filled cyan, red, brown and white circles show the Ti, O, C and H atoms, respectively. The hollow green circles show the site of the O-vacancy (without the vacancy, there should be two O atoms inside the circle). The green contour shows the electron charge loss, and the blue contour shows the electron charge gain induced by the surface binding. In this charge transfer interaction, the Ti atom changes from a 3+ to a 4+ oxidation state, and the furfuraldehyde molecule acquires a negative charge. This negative charge localizes around the carbonyl C, activating it for H addition.

UV-cleaned Pt/TiO_2 catalyst. However, in the case of a free furfuraldehyde molecule (not bound to the TiO_2 surface), there is an energy cost of 2.3 eV for a H atom from the Pt surface to bind to the carbonyl C of a furfuraldehyde molecule. Obviously, this is impossible from a thermodynamic point of view. Furthermore, the calculations show that furfuraldehyde does not bind with a SiO_2 surface. This is in accordance with the experimental observation that the Pt/SiO_2 catalyst is not SMSI active.

4. CONCLUSIONS

For furfuraldehyde hydrogenation on supported Pt, the oxide support plays a major role to determine the activity and selectivity of the catalyst. This effect, which is common to many reactions, is often referred to as a strong metal−support interaction, but a molecular-level understanding has been lacking notwithstanding the obvious scientific and practical importance. We demonstrate that when Pt nanoparticles make close contact with a TiO_2 support, the Pt/TiO_2 interface results in a new reaction pathway that is highly selective toward furfuryl alcohol formation. SFG vibrational spectroscopy shows that a furfuryl-oxy intermediate forms on TiO_2 and is the selective precursor to furfuryl alcohol. The role of the Pt/TiO_2 interface is simply to enable H spillover to this active intermediate, and this reaction pathway is ∼10 faster than the reaction rate on Pt alone. DFT calculations suggest that the formation of the active furfuryl-oxy intermediate is the result of a charge-transfer interaction between the furfuraldehyde molecule and an O-vacancy site on the TiO_2 surface. In this charge transfer interaction, the furfuraldehyde molecule acquires a negative charge that localizes around the carbonyl C, activating it for H addition. These results provide a detailed picture of the molecular and electronic interactions that combine to create the SMSI phenomenon and demonstrate that acid−base interactions are the foundation for highly selective catalysis at the oxide−metal interface.

AUTHOR INFORMATION

Corresponding Author

somorjai@berkeley.edu; lrbaker@berkeley.edu

Notes

The authors declare no competing financial interest.

ACKNOWLEDGMENTS

This work was funded by the Director, Office of Science, Office of Basic Energy Sciences of the U.S. Department of Energy under Contract No. DE-AC02-05CH11231.

REFERENCES

(1) Schwab, G. M. *Trans. Faraday Soc.* **1946**, *42*, 689.
(2) Tauster, S. J.; Fung, S. C.; Garten, R. L. *J. Am. Chem. Soc.* **1978**, *100*, 170.
(3) Tauster, S. J.; Fung, S. C.; Baker, R. T. K.; Horsley, J. A. *Science* **1981**, *211*, 1121.
(4) Tauster, S. J. *Acc. Chem. Res.* **1987**, *20*, 389.
(5) Oh, S. H.; Eickel, C. C. *J. Catal.* **1988**, *112*, 543.
(6) Zhu, H.; Qin, Z.; Shan, W.; Shen, W.; Wang, J. *J. Catal.* **2004**, *225*, 267.
(7) Chen, M. S.; Goodman, D. W. *Science* **2004**, *306*, 252.
(8) Goodman, D. *Catal. Lett.* **2005**, *99*, 1.
(9) Baker, L. R.; Hervier, A.; Seo, H.; Kennedy, G.; Komvopoulos, K.; Somorjai, G. A. *J. Phys. Chem. C* **2011**, *115*, 16006.
(10) Boffa, A. B.; Bell, A. T.; Somorjai, G. A. *J. Catal.* **1993**, *139*, 602.
(11) Boffa, A.; Lin, C.; Bell, A. T.; Somorjai, G. A. *J. Catal.* **1994**, *149*, 149.
(12) Yamada, Y.; Tsung, C.-K.; Huang, W.; Huo, Z.; Habas, S. E.; Soejima, T.; Aliaga, C. E.; Somorjai, G. A.; Yang, P. *Nat. Chem.* **2011**, *3*, 372.
(13) Vannice, M. A.; Sen, B. *J. Catal.* **1989**, *115*, 65.
(14) Lin, S. D.; Sanders, D. K.; Albert Vannice, M. *Appl. Catal. A: General* **1994**, *113*, 59.
(15) Kijeński, J.; Winiarek, P. *Appl. Catal. A: General* **2000**, *193*, L1.
(16) Malathi, R.; Viswanath, R. P. *Appl. Catal. A: General* **2001**, *208*, 323.
(17) Kijeński, J.; Winiarek, P.; Paryjczak, T.; Lewicki, A.; Mikołajska, A. *Appl. Catal. A: General* **2002**, *233*, 171.
(18) Bracey, J. D.; Burch, R. *J. Catal.* **1984**, *86*, 384.
(19) Sachtler, W. M. H.; Shriver, D. F.; Hollenberg, W. B.; Lang, A. F. *J. Catal.* **1985**, *92*, 429.
(20) Sachtler, W. M. H.; Ichikawa, M. *J. Phys. Chem.* **1986**, *90*, 4752.
(21) Jencks, W. P. *Acc. Chem. Res.* **1980**, *13*, 161.
(22) Greeley, J.; Norskov, J. K.; Mavrikakis, M. *Annu. Rev. Phys. Chem.* **2002**, *53*, 319.
(23) Olah, G. A.; Molnar, A. *Hydrocarbon Chemistry*, 2nd ed.; John Wiley & Sons, Inc.: Hoboken, NJ, 2003.
(24) Bratlie, K. M.; Kliewer, C. J.; Somorjai, G. A. *J. Phys. Chem. B* **2006**, *110*, 17925.
(25) Bratlie, K. M.; Komvopoulos, K.; Somorjai, G. A. *J. Phys. Chem. C* **2008**, *112*, 11865.
(26) Kliewer, C. J.; Bieri, M.; Somorjai, G. A. *J. Am. Chem. Soc.* **2009**, *131*, 9958.
(27) Kliewer, C. J.; Aliaga, C.; Bieri, M.; Huang, W.; Tsung, C.-K.; Wood, J. B.; Komvopoulos, K.; Somorjai, G. A. *J. Am. Chem. Soc.* **2010**, *132*, 13088.
(28) Aliaga, C.; Park, J. Y.; Yamada, Y.; Lee, H. S.; Tsung, C.-K.; Yang, P.; Somorjai, G. A. *J. Phys. Chem. C* **2009**, *113*, 6150.
(29) Kuhn, J. N.; Huang, W.; Tsung, C.-K.; Zhang, Y.; Somorjai, G. A. *J. Am. Chem. Soc.* **2008**, *130*, 14026.
(30) Song, H.; Kim, F.; Connor, S.; Somorjai, G. A.; Yang, P. *J. Phys. Chem. B* **2004**, *109*, 188.
(31) Schlatter, J. C.; Boudart, M. *J. Catal.* **1972**, *24*, 482.
(32) Kuhn, J. N.; Tsung, C.-K.; Huang, W.; Somorjai, G. A. *J. Catal.* **2009**, *265*, 209.

(33) Pushkarev, V.; Musselwhite, N.; Ann, K.; Alayoglu, S.; Somorjai, G. *Nano Lett.* **2012**, submitted.
(34) Krier, J. M.; Michalak, W. D.; Baker, L. R.; An, K.; Komvopoulos, K.; Somorjai, G. A. *J. Phys. Chem. C* **2012**, submitted.
(35) Seo, H.; Baker, L. R.; Hervier, A.; Kim, J.; Whitten, J. L.; Somorjai, G. A. *Nano Lett.* **2010**, *11*, 751.